Heliyon 9 (2023) e19975

Contents lists available at ScienceDirect

Heliyon

journal homepage: www.cell.com/heliyon

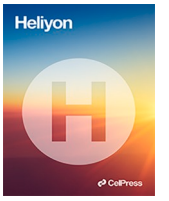

Identification of EGFR as an essential regulator in chondrocytes ferroptosis of osteoarthritis using bioinformatics, *in vivo*, and *in vitro* study

Hong Sun [a,b,c,1], Guoxuan Peng [a,1], Kunhao Chen [a,c], Zhilin Xiong [a,c], Yong Zhuang [a], Miao Liu [a], Xu Ning [a], Hua Yang [a,**], Jin Deng [b,c,*]

[a] *Department of Orthopaedics, The Affiliated Hospital of Guizhou Medical University, Guiyang, 550004, China*
[b] *Department of Emergence Surgery, The Affiliated Hospital of Guizhou Medical University, Guiyang, 550004, China*
[c] *School of Clinical Medicine, Guizhou Medical University, Guiyang, 550004, China*

ARTICLE INFO

Keywords:
Osteoarthritis
Ferroptosis
Biomarkers
Ferroptosis related patterns
Competing endogenous RNA
EGFR

ABSTRACT

Objective: The mechanisms of chondrocytes ferroptosis in osteoarthritis (OA) have not yet been fully elucidated. This study aimed to identify key ferroptosis related genes (FRGs) involved in chondrocytes ferroptosis.

Methods: LASSO, SVM-RFE, and receiver operating characteristic curve (ROC) were performed to screen key differentially expressed FRGs (DEFRGs). Functional analyses were conducted using GO, and KEGG analyses. Unsupervised clustering analysis was used to identify ferroptosis related patterns. The CeRNA network was constructed to predict the upstream miRNAs and lncRNAs. Finally, we validated the role of EGFR in chondrocytes ferroptosis using *in vivo* and *in vitro* experiments.

Results: A total of 42 DEFRGs were identified between OA and normal cartilages. GO and KEGG analyses indicated that these DEFRGs were significantly engaged in ferroptosis related biological processes and pathways, such as cellular response to oxidative stress, positive regulation of programmed cell death, MAPK and PI3K-Akt signaling pathways. Moreover, four key DEFRGs, including ACSF2, AURKA, EGFR, and KLHL24, were considered as potential biomarkers of OA. Moreover, two distinct ferroptosis related patterns were determined, and a total of 882 differentially expressed genes were identified which might participate in extracellular matrix degradation and inflammatory response. In addition, the CeRNA network showed that EGFR could be competitively regulated by 3 lncRNAs and 4 miRNAs. Significantly, the expression of EGFR was downregulated in human OA cartilages, OA mouse model, and erastin induced chondrocytes. EGFR inhibition could induce the occurrence of chondrocytes ferroptosis and ECM degradation which could be reversed by the addition of Ferrostatin-1.

Conclusion: Our study has identified ACSF2, AURKA, EGFR, and KLHL24 as ferroptosis-related biomarkers in OA. Furthermore, we have conducted a preliminary investigation into the role of EGFR in regulating chondrocytes ferroptosis. These findings offer novel insights into the molecular mechanisms underlying OA.

* Corresponding author. Department of Emergence Surgery, The Affiliated Hospital of Guizhou Medical University, Guiyang, 550004, China.
** Corresponding author. Department of Orthopaedics, The Affiliated Hospital of Guizhou Medical University, Guiyang, 550004, China.
E-mail addresses: yanghua0203@gmc.edu.cn (H. Yang), gydengjin@yeah.net (J. Deng).
[1] Hong Sun and Guoxuan Peng contributed equally to this study.

https://doi.org/10.1016/j.heliyon.2023.e19975
Received 12 June 2023; Received in revised form 5 September 2023; Accepted 7 September 2023
Available online 9 September 2023

1. Introduction

Osteoarthritis (OA) is a prevalent chronic joint disease which is mainly characterized by joint pain and limited movement [1]. It is estimated that 300 million people worldwide are currently suffering from OA, and its incidence is gradually increasing [2,3]. The pathological features of OA include loss of articular cartilage, abnormality of subchondral bone remodeling, synovial hyperplasia and angiogenesis, and osteophytes formation [4]. Until now, the effective therapy to inhibit the progression of OA is still limited. It is shown that cartilage degeneration serves as a key factor in the pathogenesis of OA [5]. As the sole cell type in articular cartilage, chondrocytes are responsible for the maintenance of cartilage homeostasis and integrity [6]. Increasing studies have demonstrated that programmed cell death of chondrocytes, including apoptosis, necrosis, pyroptosis, and ferroptosis, can contribute to the development of OA [7–9]. Therefore, targeting chondrocytes death may be a potential strategy for the treatment of OA.

Ferroptosis is an iron-dependent type of cell death that was firstly described by Dixon et al., in 2012, and is usually accompanied by large amount of iron accumulation and lipid peroxidation [10]. Compelling studies have demonstrated that a redox imbalance between the production of oxidants and antioxidants driven by the dysfunction of multiple redox-active enzymes contributes to the occurrence and development of ferroptosis [11,12]. Furthermore, two major pathways are reported involving in the pathogenesis of ferroptosis, including the extrinsic or transporter-dependent pathway and the intrinsic or enzyme-regulated pathway [12]. Recently, ferroptosis has recently been found implicating in multiple diseases, including OA. It was reported that iron could trigger the early stages of bovine articular cartilage degeneration *in vitro* by enhancing the release of sulfated glycosaminoglycans [13]. Yao et al. demonstrated that both inflammation and iron overload condition could lead to chondrocytes ferroptosis, and intraarticular injection of a ferroptosis inhibitor could reverse the downregulation of collagen II and upregulation of matrix metalloproteinase 13 (MMP13), thereby attenuating the cartilage degradation [14]. As a suppressor of inflammation and allergy, it was shown that Baicalein could inhibit chondrocytes ferroptosis, and thus alleviate OA development via activating AMPK/Nrf2/HO-1 signaling pathway [15]. These findings indicate that inhibition of ferroptosis may be a promising treatment option for OA. However, the underlying mechanisms of ferroptosis in the progression of OA remain largely unknown. Hence, it is of great significance to investigate the role of ferroptosis related genes (FRGs) in regulating chondrocytes ferroptosis.

In this study, we used multiple bioinformatics analyses to identify key differentially expressed FRGs (DEFRGs), and investigated their involved biological functions, and regulatory mechanisms. Finally, the role of EGFR in chondrocytes ferroptosis was further confirmed using *in vivo*, and *in vitro* experiments. These findings may shed new light on the molecular mechanisms of OA, and further provide diagnostic biomarkers and therapeutic targets for OA.

2. Materials and methods

2.1. Data sources

A total of 259 FRGs, which are regulators and markers of ferroptosis, were obtained from the FerrDb database (http://www.zhounan.org/ferrdb/current/). The dataset GSE117999 which contains 10 OA and 10 normal cartilage samples was obtained from the Gene Expression Omnibus (GEO) database. In addition, GSE114007 dataset which contains 20 OA and 18 non-OA cartilage samples was used as an external dataset to validate the expression and diagnostic values of candidate DEFRGs. The clinical information of patients in two datasets is shown in Supplementary Table S1.

2.2. Identification and functional enrichment analysis of DFRGs between OA and normal cartilage samples

The student's t-test was used to compare the expression of FRGs between OA and normal cartilages in GSE117999 dataset. The DEFRGs were screened with P value < 0.05. Subsequently, we used the ClusterProfiler R package to analyze the enriched biological processes (BPs) and pathways of DEFRGs. To improve the biological interpretation of DEFRGs, we used ClueGo plug-in to build a functionally organized Gene Ontology (GO)/pathway term network, which integrated GO terms as well as Kyoto Encyclopedia of Genes and Genomes (KEGG) and Reactome pathways.

2.3. Interactions among DEFRGs

To explore the interactions among DEFRGs, a protein-protein interaction (PPI) network was constructed using the STRING database and Cytoscape software (version 1.6.20). Furthermore, a plug-in of Cytoscape software Molecular Complex Detection (MCODE) was used to screen the significant modules in PPI network. The screening parameter was set as Node Score Cutoff = 0.2, Haircut = true, Fluff = false, K-Core = 2, and Max Depth from Seed = 100. Furthermore, the correlations between DEFRGs in OA patients were investigated by the R package "corrplot" and Spearman's correlation analysis.

2.4. Selection of candidate DEFRGs by LASSO and SVM-RFE algorithms

The LASSO algorithm was applied using the glmnet package in R software (version 4.0.0) with penalty parameter tuning conducted by 5-fold cross-validation, and feature DEFRGs were selected under the optimal lambda with the smallest classification error. SVM-RFE was performed using the e1071 package in R software (version 4.0.0) to screen feature DEFRGs by deleting SVM-generated

eigenvectors in conjunction with 10-fold cross-validation. Finally, Venn diagram analysis was conducted to determine the candidate DEFRGs between LASSO and SVM-RFE algorithms.

2.5. Recognition of ferroptosis related patterns

Unsupervised clustering analysis was conducted to determine distinct ferroptosis related patterns based on the expression level of screened key DEFRGs. The "ConsensusClusterPlus" software was used to categorize OA patients into distinct subtypes, and the principal component analysis (PCA) was conducted to access the ferroptosis related patterns. Differentially expressed genes (DEGs) between two distinct subtypes were screened with $Log_2FC \geq 1$ and P value < 0.05. GO enrichment and KEGG pathway analyses were performed to identify enriched BPs and pathways of DEGs.

2.6. Construction of the competing endogenous RNA (ceRNA) network

Differentially expressed long non-coding RNAs (lncRNAs) were identified from the GSE117999 dataset (P value < 0.05). The miRanda software (version 3.3a) was used to predict the microRNAs (miRNAs) targeting key DEFRGs and interacting with differentially expressed lncRNAs. The combined score >500 and minimum free energy (MFE) < -400 were set as the screening criteria of lncRNA-miRNA. Meanwhile, the parameter was set as combined score >500 and MFE < -100 for screening miRNA-mRNA. Accordingly, miRNA-mRNA and lncRNA-miRNA pairs were obtained. The miRNAs shared in the lncRNA-miRNA and miRNA-mRNA pairs were used to construct a lncRNA-miRNA-mRNA network, which was further visualized using the Cytoscape software (version 1.6.20).

2.7. Human cartilage samples collection

This study was designed in accordance with the Declaration of Helsinki and was approved by the ethics committee of the Affiliated Hospital of Guizhou Medical University (No. 276 in 2022). A total of 6 OA cartilages were obtained from patients undergoing total knee arthroplasty, and 5 normal cartilages of femoral heads were acquired from patients with no previous history of OA or rheumatoid arthritis, who underwent total hip arthroplasty because of hip fractures. The X ray image used in current study has been consented for publication from patients. The clinical information of these patients is listed in Supplementary Table S2. Notably, damaged samples were collected from areas with gross erosion, while undamaged samples were collected from areas with regular surface of OA knee cartilage. The damaged and undamaged samples were used for further histological and immunofluorescence staining. In addition, OA and normal cartilages were frozen with liquid nitrogen and ground with a mortar and pestle [16]. The extracts were prepared for total RNA isolation.

2.8. Animal experiments

The protocol of animal experiments in this study was approved by the institutional Animal Care and Use Committee of Guizhou Medical University (No.2201177). Eight-week-old male C57BL/6 J mice (n = 6) weighing 20–25 g were purchased from the Experimental Animal Center of Guizhou Medical University (Guiyang, China). The experimental OA model was constructed by surgical destabilization of the medial meniscus (DMM) in the left knee joint. Briefly, after anesthetized with pentobarbital (35 mg/kg) intraperitoneally, the left knee joint of mice was exposed and then the medial meniscotibial ligament was transected. Finally, the joint capsule and skin were closed. As a control, sham operation was performed on the right knee joint with medial capsulotomy only. The mice were sacrificed at 8 weeks after DMM or sham surgery. The knee samples were collected and fixed in 4% paraformaldehyde for further investigation.

2.9. Histology and immunofluorescence staining

After decalcification in 10% EDTA at pH 7.4 for 2 weeks, the knee samples were dehydrated with gradient ethanol, embedded in paraffin, and sectioned into slices of 5 μm thickness in a sagittal plane. Afterwards, sections of human and mice cartilages were undergone with Safranin O/Fast Green staining. The Osteoarthritis Research Society International (OARSI) score system was applied to evaluate the severity of cartilage degeneration in DMM OA mouse model. For immunofluorescence staining, paraffin sections of human and mice cartilages were rehydrated. Sections were pre-treated with 3% H_2O_2 for 10 min at room temperature, and then incubated with Trypsin Induced Antigen Retrieval Solution for 45 min at 37 °C. Next, the slides were permeabilized with 0.5% Triton X-100 in phosphate buffered saline (PBS) for 10 min and rinsed twice with PBS for 5 min each, and then blocked with 10% donkey serum (SL050, Solarbio) in PBS for 1 h at 37 °C. Paraffin sections were incubated with primary antibodies, including *anti*-GPX4 (1:100, No. 67763-1-Ig, Proteintech), and *anti*-EGFR (1:150, ab52894, Abcam) overnight at 4 °C. After the sections were washed three times with PBS, the slides were incubated with secondary antibody of Donkey Anti-Rabbit IgG H&L (Alexa Fluor® 594) preadsorbed (1:800, ab150064, Abcam) for preadsorption, and nuclear counterstaining was performed using DAPI. The samples were then mounted with 50% glycerin, and images were acquired using a confocal microscopy (Leica SP5, Germany).

2.10. Isolation and culture of mouse chondrocytes

Primary mouse chondrocytes were isolated from 5-7-day-old C57BL/6 J mice as described before [17]. Briefly, articular cartilages were removed and dissected into pieces. The cartilages were digested with 3 mg/ml collagenase D (Roche® Life Science Products, 11088858001) for 45 min, followed by 0.5 mg/ml collagenase D for overnight at 37 °C. The primary chondrocytes were cultured in DMEM/F12 medium (Gibco, C11330500BT) containing 10% fetal bovine serum (Gibco, 10099141), 1% penicillin and 1% streptomycin sulfate at 37 °C with 5% CO_2. Chondrocytes at second passage were used in present study.

2.11. Cell viability assay

Chondrocytes viability was detected using the cell counting kit-8 (CCK-8, meilunbio, MA0218). Chondrocytes were seeded into 96-well plates with at a density of 5000 cells per well. After adherence for 24 h, cells were treated with erastin (APExBIO, B1524) (0, 0.25, 0.5, 1, 2.5, and 5 μM), or gefitinib (APExBIO, A8219) (0, 2.5, 5, 10, 25, and 50 μM) for 24 h. After removal of culture medium, 100 μl of 10% CCK-8 solution was added into each well, and incubated for at 37 °C away from light for 2 h. The absorbance at 450 nm was measured using a microplate reader (Elx800 bio-tek instruments, USA).

2.12. Toluidine blue staining

Toluidine blue staining (Solarbio, G3660) was adopted to analyze the morphology change of chondrocytes according to the manufacturer's instructions. In brief, chondrocytes were seeded in 12-well plates at a density of 1.5×10^5 cells/well. After adherence for 24 h, cells were treated with gefitinib (0, 2.5, 5, 10, 25, and 50 μM) for 24 h. Subsequently, cells were gently stained with toluidine blue for 5min at room temperature. Equal volume of distilled water was added into wells, and cells were stained for another 15 min. Finally, cells were washed twice with PBS, and were observed using a microscope (Nikon Eclipse TE2000-U, Japan)

2.13. Detection of intracellular ROS and lipid-ROS

In brief, chondrocytes were seeded in 24-well plates at a density of 1×10^5 cells/well, and 15 mm-well at a density of 1.5×10^5 cells/well, respectively. After different treatments, cells were incubated with 10 μM DCFH-DA (Beyotime Biotech, China, S0033S), or 1 μM C11-BODIPY$^{581/591}$ (Thermo Fisher Scientific, D3861) for 30 min at 37 °C in the dark. After incubation, cells were washed with serum-free medium and observed under the fluorescence microscope (Nikon Eclipse TE2000-U, Japan), and confocal microscope (Leica SP5, Germany), respectively.

2.14. Transmission electron microscopy

Chondrocytes were seeded into T25 culture flasks, and stimulated with different treatments for 24 h. Cells were harvested and fixed with 2.5% glutaraldehyde (Servicebio, G1102) for 30 min at room temperature in the dark. Subsequently, cells were washed with PBS three times, and dehydrated in a graded series of alcohol (50%, 70%, 80%, 90%, 95%, and 100%). After embedding, section, and staining, ultrastructural images of the chondrocytes were observed using a transmission electron microscope (Hitachi HT7800, Japan).

2.15. Real-time PCR analysis

Chondrocytes were seeded into 12-well plates at a density of 1.5×10^5 cells/well. After adherence for 24 h, cells were treated with erastin (0, 1, and 2.5 μM), or Gefitinib (0, and 10 μM) for 24 h. Total RNA of articular cartilages and cells was isolated using TRIzol reagent (Thermo Fisher Scientific, 15596026) according to the manufacturer's instructions, and the Nanodrop 2000 (Thermo Scientific, USA) was applied to quantify the RNA. Subsequently, 500 ng of total RNA reverse transcribed into complementary DNA sequences using PrimeScript™ RT Master Mix (Takara Bio Inc., RR036A), and qRT-PCR was conducted on a BioRad CFX96 using the TB Green® Premix Ex Taq™ II (Takara Bio Inc., RR820A)) according to the manufacturer's instructions. The relative expression of mRNA was calculated using the method of $2^{-\Delta\Delta Ct}$ based on the GAPDH. The primer sequences are shown in Table 1.

Table 1
The primer sequences used in the study.

Gene	Forward	Reverse
Has-EGFR	5′-TTGCCGCAAAGTGTGTAACG-3′	5′-GTCACCCCTAAATGCCACCG-3′
Has-GAPDH	5′-CAGGAGGCATTGCTGATGAT-3′	5′-GAAGGCTGGGGCTCATTT-3′
Mmu-EGFR	5′-GCATCATGGGAGAGAACAACA-3′	5′- CTGCCATTGAACGTACCCAGA-3′
Mmu-Col2a1	5′-CCCGCCTTCCCATTATTGAC-3′	5′- GGGAGGACGGTTGGGTATCA-3′
Mmu-MMP13	5′-ATGCATTCAGCTATCCTGGCCA-3′	5′-AAGATTGCATTTCTCGGAGCCTG-3′
Mmu-GPX4	5′- GCCTGGATAAGTACAGGGGTT-3′	5′- CATGCAGATCGACTAGCTGAG-3′
Mmu-GAPDH	5′-AGGTCGGTGTGAACGGATTTG-3′	5′-TGTAGACCATGTAGTTGAGGTCA-3′

2.16. Western blot analysis

Chondrocytes in 6-well plates at a density of 5×10^5 cells/well were subjected to different treatments for 24 h. Then, cells were harvested with RIPA lysis buffer (Beyotime Biotech, P0013C) containing 1% phenylmethylsulfonyl fluoride (PMSF, Solarbio, 329-98-6) for 30 min on ice. After centrifugation at 12,000×*g* and 4 °C for 20 min, the supernatant was collected, and the concentration of protein was detected using the Nanodrop 2000 (Thermo Scientific, USA). Samples containing equal quality of extracted protein were separated in 8%, or 12% SDS-PAGE gels, and transferred to PVDF membranes (Millipore, USA). After blocking with 5% skim milk for 2 h at room temperature, membranes were incubated with primary antibodies against Collagen II (1:2000, 28459-1-AP, Proteintech), GPX4 (1:2000, 67763-1-Ig, Proteintech), EGFR (1:1000, ab52894, Abcam), MMP13 (1:1000, 18165-1-AP, Proteintech), and GAPDH (1:10000, 10494-1-AP, Proteintech) at 4 °C overnight, and then incubated with the corresponding secondary antibodies for 2 h at room temperature. Finally, protein bands were visualized using Omni-ECL™Pico Light Chemiluminescence Kit (Epizyme Biomedical Technology, China), and images were analyzed using ImageJ software.

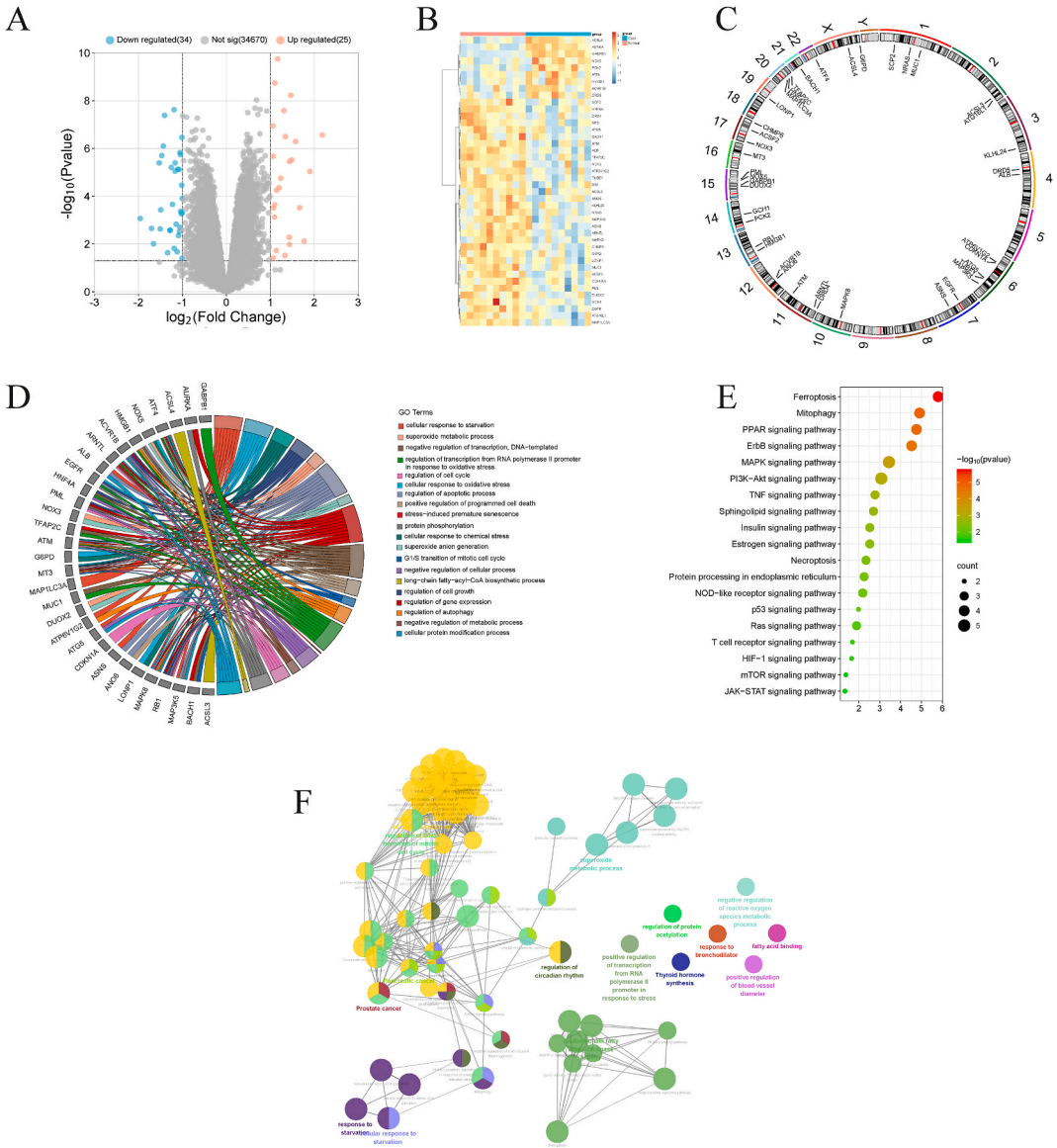

Fig. 1. Identification and function analyses of DEFRGs. (**A**) DEGs between normal and OA samples in GSE117999 dataset. (**B**) Visualizing the expression of DEFRGs between normal and OA samples using heatmap. (**C**) The location of DEFRGs on human chromosomes. (**D**) GO enrichment analysis of DEFRGs. (**E**) KEGG pathway analysis of DEFRGs. (**F**) Interactions between enriched GO and KEGG terms using ClueGO analysis.

2.17. Statistical analysis

All data of bioinformatics were analyzed using R software (version 4.0.0). The ROC curve generated by the "survivalROC" in R package was used to assess the diagnostic value of candidate DEFRGs, and the value of genes with the areas under the ROC curves (AUC) ≥ 0.7 was considered as potential biomarkers in distinguishing OA and non-OA cartilages. All *in vivo* and *in vitro* experiments were performed with at least three biological replicates. Data were described as the means ± standard error of mean (SEM), and further visualized and analyzed using GraphPad Prism (GraphPad Software, USA). The student's t-test or Mann-Whitney test were applied to compare the differences between groups depending on whether the data were normally distributed or not. One-way analysis of variance (ANOVA) and Dunnett' *t*-test were carried out for multiple group comparisons. Differences with P value < 0.05 were considered as statistical significance.

3. Results

3.1. Identification and functional analyses of DEFRGs between OA and normal cartilage samples

The expression profile of GSE117999 dataset is shown in Fig. 1A. After comparing the expression level of all FRGs in GSE117999

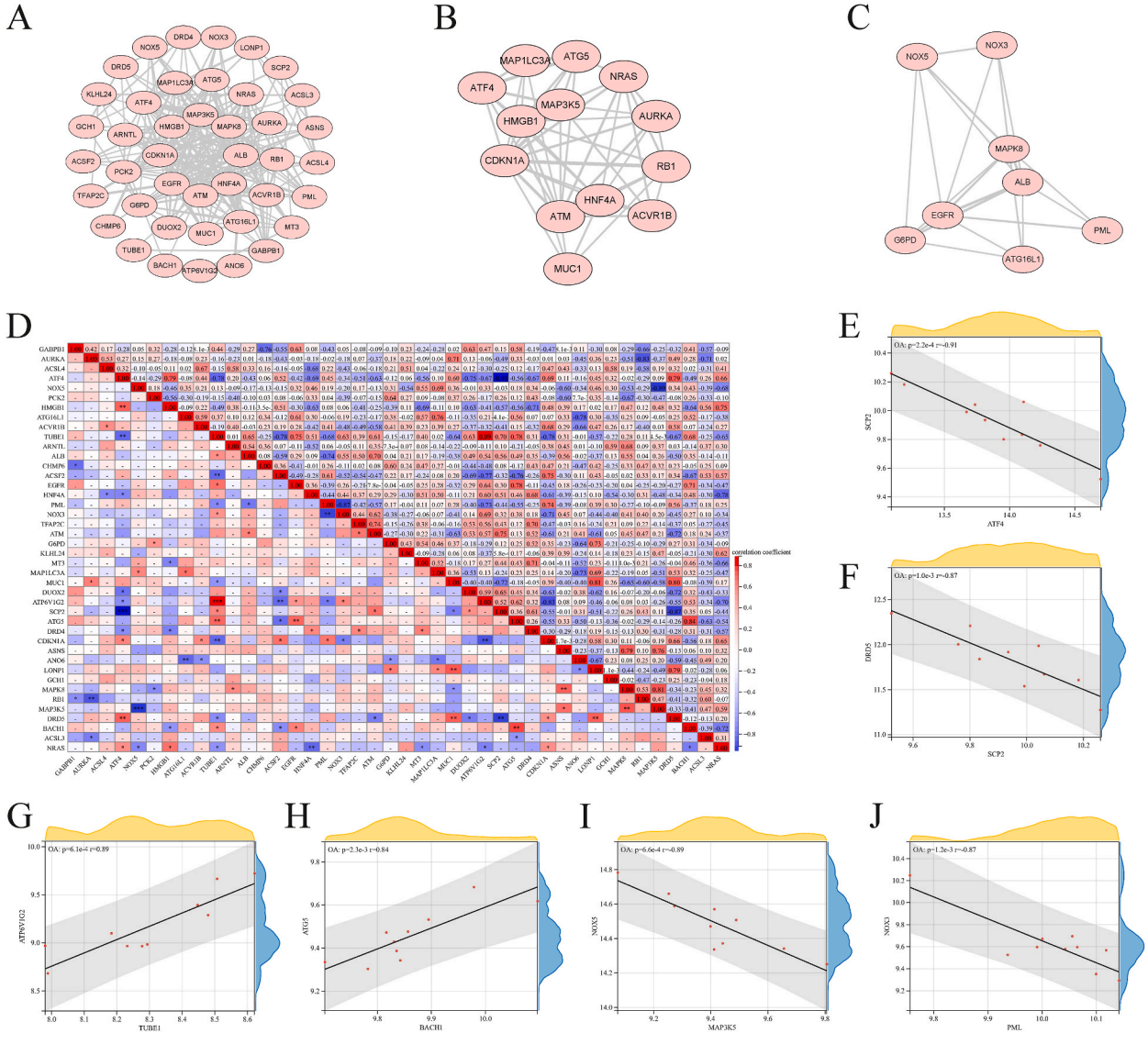

Fig. 2. Interaction analysis among DEFRGs. (**A**) PPI network of DEFRGs. (**B, C**) Two regulatory modules constructed using MCODE. (**D**) The interaction analyses of DEFRGs expression in OA samples. (**E-J**) The correlation between DEFRGs with a strong correlation coefficient.

dataset, a total of 42 DEFRGs were thus identified, in which 9 were increased, and the other 33 were decreased in OA cartilage samples (Supplementary Table S3). Heatmap visualizes the expression of these 42 DEFRGs in each sample of the GSE117999 dataset (Fig. 1B). The positions of these DEFRGs on the chromosomes are described in Fig. 1C. GO and KEGG analyses were further performed to investigate the biological functions and pathways of DEFRGs. GO analysis showed that these DEFRGs were enriched in a variety of BPs, such as regulation of cell cycle, cellular response to oxidative stress, and positive regulation of programmed cell death (Fig. 1D). KEGG analysis found that these DEFRGs were primarily engaged in the pathways including ferroptosis, MAPK, and PI3K-Akt signaling pathways (Fig. 1E). These findings indicated that DEFRGs were closely associated with ferroptosis related BPs and pathways. Furthermore, we used the ClueGO plug-in to investigate the interactions between enriched GO terms and KEGG pathways. In the network, we found that ferroptosis could interact with many metabolic-related pathways, such as the PPAR signaling pathway, adipocytokine signaling pathway, and fatty acids ligase activity (Fig. 1F), indicating that ferroptosis may be involved in OA progression by cooperation with metabolism related pathways, especially fat metabolism.

3.2. The interactions among DEFRGs

In the PPI network, these DEFRGs could directly or indirectly interacted with each other (Fig. 2A). In addition, we found two significant modules using the MCODE. 13 DEFRGs, including ATF4, MAP1LC3A, ATG5, NRAS, AURKA, RB1, ACVR1B, MUC1, ATM, HNF4A, CDKN1A, HMGB1, MAP3K5, were found as hub nodes in module 1 (Fig. 2B), and 8 DEFRGs, including NOX5, NOX3, MAPK8, ALB, G6PD, ATG16L1, PML, and EGFR, were found as hub nodes in module 2 (Fig. 2C).

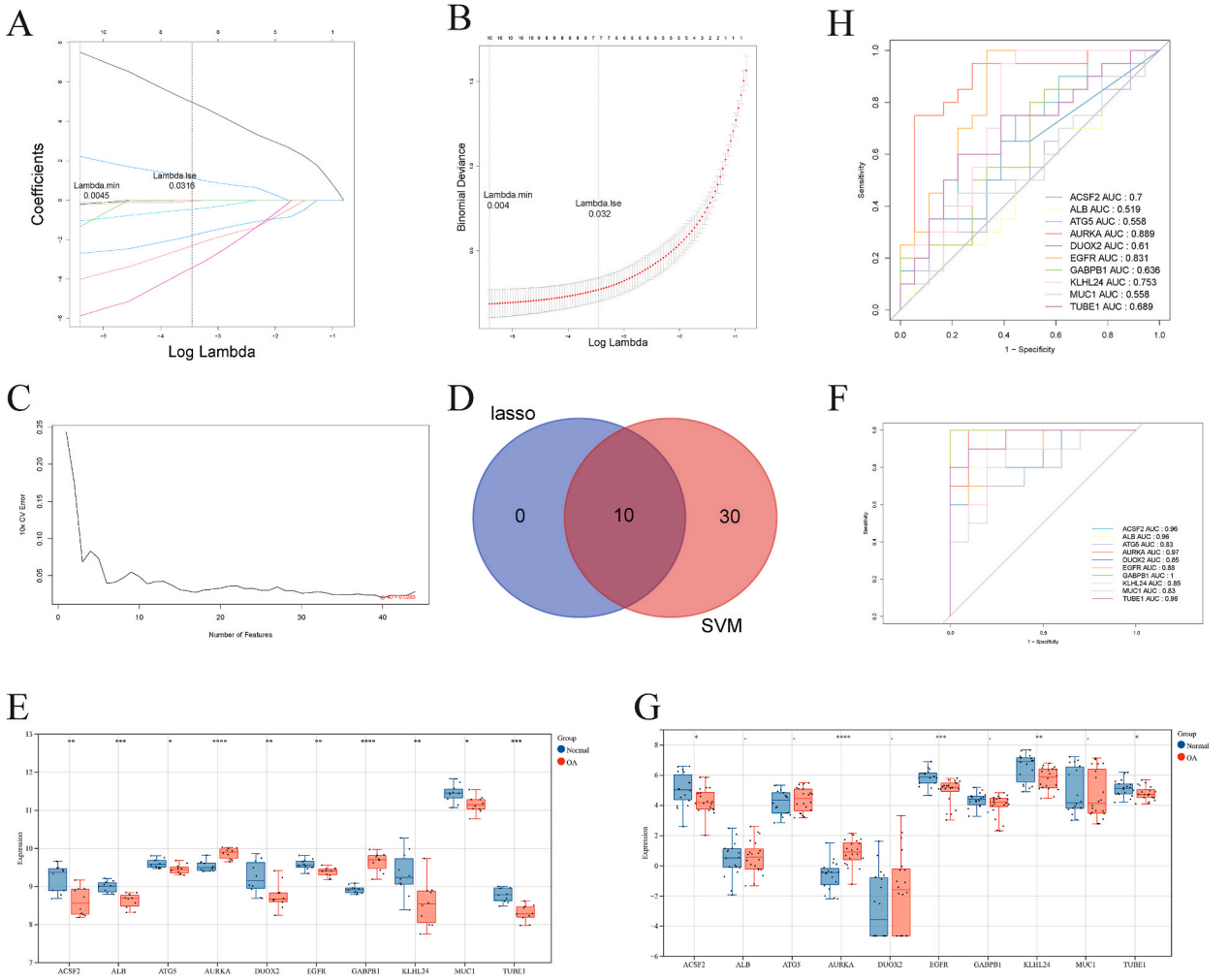

Fig. 3. Identification and validation of candidate DEFRGs. (**A**) Five-fold cross-validation applied for parameter selection in LASSO regression. (**B**) The candidate DEFRGs screened using LASSO regression. (**C**) The candidate DEFRGs identified using SVM-RFE algorithm. (**D**) Venn diagram showing the common candidate DEFRGs between LASSO and SVM-RFE algorithms. (**E**) The expression of candidate DEFRGs between normal and OA samples in GSE117999 dataset. (F) ROC curves of candidate DEFRGs in GSE117999 dataset. (G) Validation the expression of candidate DEFRGs between normal and OA samples in GSE114007 dataset. (H) ROC curves of candidate DEFRGs in GSE114007 dataset.

We further explored the correlations among these DEFRGs in the OA samples. Interestingly, multiple DEFRGs showed a significant correlation with each other (Fig. 2D). For example, the expression levels of ATF4 and DRD5 were inversely correlated with SCP2 (Fig. 2E&F), while those of TUBE and ATG5 showed positive associations with ATP6V1G2 and BACH1 (Fig. 2G&H), respectively. Conversely, the expression levels of MAP3K5 and PML were negatively associated with NOX5 and NOX3 (Fig. 2I&J), respectively.

3.3. Identification and validation of key DEFRGs in OA

Both LASSO and SVM-RFE algorithms were used to screen candidate DEFRGs. Ten and 40 DEFRGs were identified using the LASSO and SVM-RFE algorithms, respectively (Fig. 3A–C). Venn diagram depicts the overlapping DEFRGs between these two algorithms (Fig. 3D). Finally, 10 DEFRGs including ACSF2, ALB, ATG5, AURKA, DUOX2, EGFR, GABPB1, KLHL24, MUC1, TUBE1, were identified as candidate DEFRGs in OA. The expression of AURKA and GABPB1 was significantly elevated, while the expression of the other eight DEFRGs was remarkably reduced in OA samples (Fig. 3E). The diagnostic values of these 10 candidate DEFRGs were assessed using ROC curve analysis. The AUC value was 0.96, 0.96, 0.83, 0.97, 0.85, 0.88, 1, 0.85, 0.83, and 0.96 for ACSF2, ALB, ATG5, AURKA, DUOX2, EGFR, GABPB1, KLHL24, MUC1, and TUBE1, respectively (Fig. 3F). Moreover, we further validated their expression and AUC

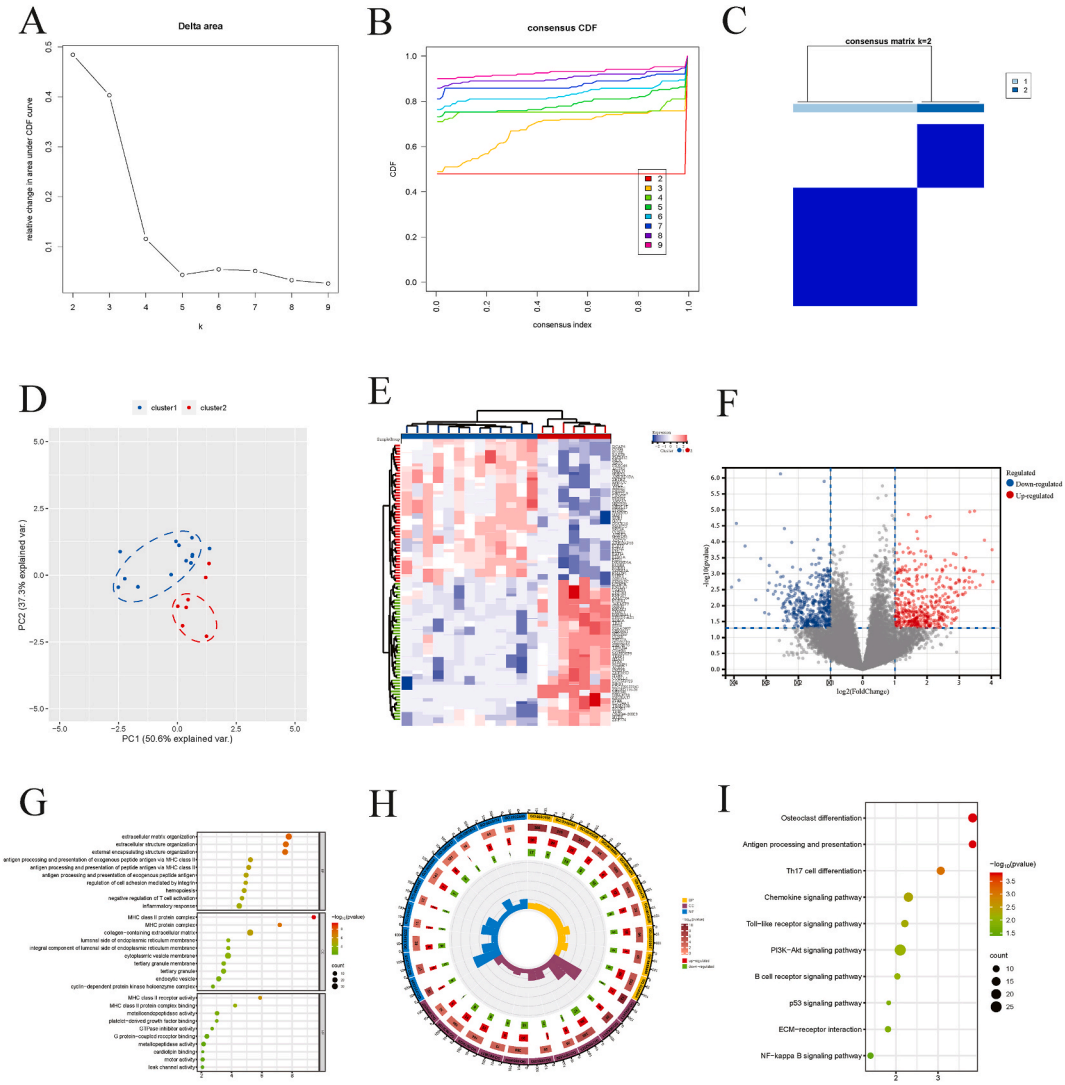

Fig. 4. Two distinct ferroptosis related patterns in OA. (**A**) The delta area difference for $k = 2$–9. (**B**) Change of the area under the cumulative distribution function (CDF) curve for k from 2 to 9. **(C)** Consensus clustering matrix with $k = 2$. (**D**) PCA analysis depicting two distinct clusters of OA samples in GSE114007 dataset. (**E**) Heatmap of ferroptosis pattern related DEGs between two clusters. (**F**) Volcano plots displaying the ferroptosis pattern related DEGs (Fold change $\geq$2 and $P < 0.05$). (**G**) GO enrichment analysis of ferroptosis pattern related DEGs from three perspectives: BP, CC, and MF. (**H**) The circle diagram of gene enrichment numbers for each GO item. (**I**) KEGG pathway analysis of ferroptosis pattern related DEGs.

values to get more robust performances in the diagnosis of OA using an external GSE114007 dataset. We found that the expression trends of ACSF2, AURKA, EGFR, KLHL24 and TUBE1 were consistent with those in GSE117999 dataset (Fig. 3G), and the AUC values of ACSF2, AURKA, EGFR and KLHL24 were ≥0.7 (Fig. 3H), indicating that ACSF2, AURKA, EGFR and KLHL24 are key DEFRGs in OA, and have robust performances in distinguishing OA and non-OA cartilage samples.

3.4. Different ferroptosis related patterns distinguished by key DEFRGs in OA

Using unsupervised clustering analysis, OA cartilage samples in GSE114007 dataset were categorized into several genetic subgroups in according to key DEFRGs. The delta area of the curve, the consensus cumulative distribution function (CDF), and consensus matrix heatmap were used to evaluate the clustering stability with *k* values from 2 to 9 (Fig. 4A&B; Supplementary Figure S1). The optimal *k* value was 2, and thus OA cartilage samples were separated into two distinct ferroptosis related patterns (Fig. 4C). PCA analysis suggested that OA samples could be categorized into two clusters, and there were 13 cases in cluster 1 and 7 cases in cluster 2 (Fig. 4D). A total of 882 DEGs were recognized between two clusters, in which 427 genes were upregulated, and 455 genes were downregulated (Fig. 4E&F; Supplementary Table S4). GO analysis was conducted to analyze the biological functions of ferroptosis pattern related DEGs from three perspectives including BP, cellular composition (CC), and molecular function (MF) (Fig. 4G&H). These DEGs were significantly associated with extracellular matrix organization, and inflammatory response, in terms of BP; collagen-containing extracellular matrix, and lumenal side of endoplasmic reticulum membrane, in terms of CC; MHC class II receptor activity, and metalloendopeptidase activity, in terms of MF. KEGG analysis showed that the ferroptosis pattern related DEGs were remarkably enriched in multiple pathways, such as Th17 cell differentiation, PI3K-Akt, and NF-κB signaling pathways (Fig. 4I).

3.5. Construction of ceRNA regulatory network

LncRNAs can act as sponges by binding to miRNAs and further regulate the expression of corresponding mRNAs. Thus, we constructed a lncRNA-miRNA-mRNA regulatory network to explore the role of lncRNAs and miRNAs in regulating the expression of key DEFRGs. We identified 469 differentially expressed lncRNAs in GSE117999 dataset (Supplementary Table S5). Heatmap depicts the expression of top 25 up-regulated and top 25 down-regulated lncRNAs (Fig. 5A). Consequently, only EGFR, one of key DEFRGs, was screened for constructing the ceRNA network (Fig. 5B). Significantly, 3 lncRNAs (LINC00265, LINC00051, and KCTD21-AS) and 4 miRNAs (has-miR-6846–5p, has-miR-4763–3p, has-miR-6796–5p, and has-miR-6860) could competitively regulate the expression of EGFR, respectively. In addition, we investigated the potential roles of lncRNA-miRNA-EGFR networks in the pathogenesis of OA using

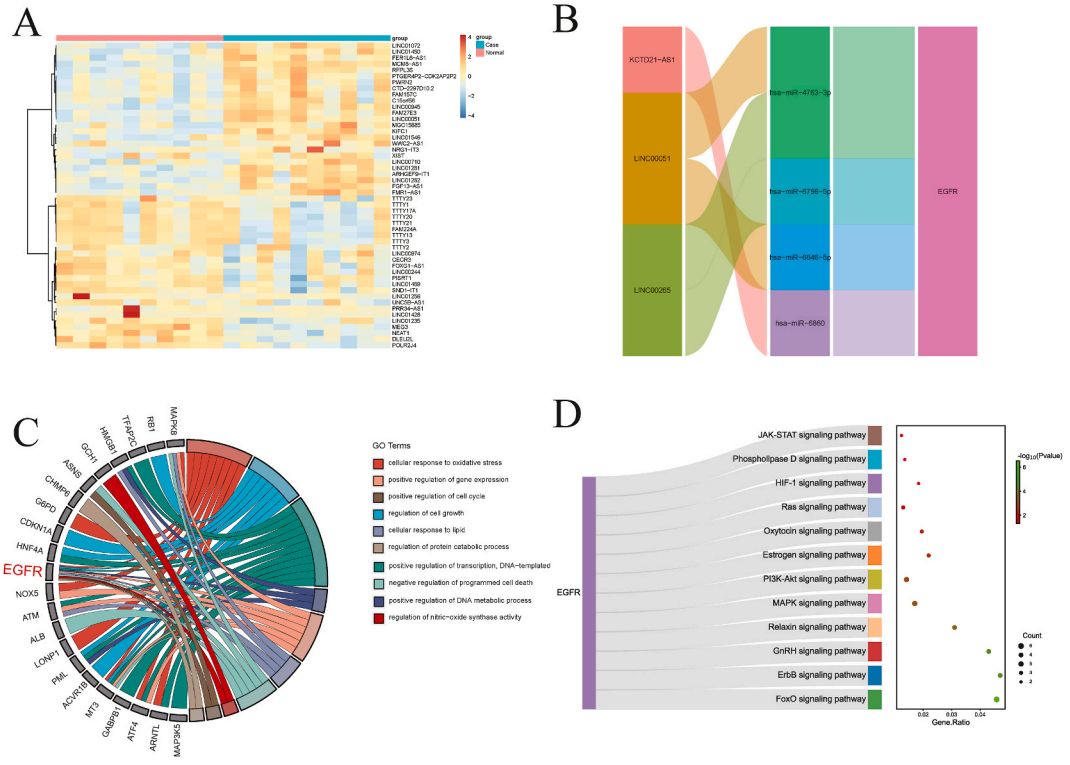

Fig. 5. Construction ceRNA network based on key DEFRGs. (**A**) Heatmap of differentially expressed lncRNAs between OA and normal samples in GSE117999 dataset. (**B**) CeRNA regulatory network composed by lncRNAs, miRNAs and EGFR. (**C**) GO enrichment analysis indicating the EGFR related BPs. (**D**) KEGG analysis revealing the EGFR involved signaling pathways.

GO and KEGG analyses. GO analysis showed that EGFR was remarkably associated with cellular response to oxidative stress, cellular response to lipid, and negative regulation of programmed cell death (Fig. 5C). In addition, KEGG analysis indicated EGFR was engaged in the regulation of MAPK, PI3K-Akt, and JAT-STAT signaling pathways (Fig. 5D). Hence, we speculated that these lncRNA-miRNA-EGFR networks may participate in the development of OA though regulating ferroptosis related BPs and pathways.

3.6. The expression of EGFR in human normal and OA cartilages

To determine the potential involvement of EGFR in the progression of OA, we initially collected cartilage samples from one patient who underwent TKA, and divided them into undamaged and damaged cartilage tissues (Fig. 6A). The integrity of superficial layer was assessed using Safranin-O/Fast Green staining, and the results showed that the undamaged cartilage was relatively smooth, whereas the damaged cartilage got erosion (Fig. 6B). We also visualized the expression of EGFR in undamaged and damaged cartilages by immunofluorescence staining. The results indicated that the number of EGFR positive cells was reduced in damaged cartilage (Fig. 6C). Subsequently, we compared the expression of EGFR between normal and OA cartilages. As shown in Fig. 6D, the mRNA level of EGFR was significantly downregulated in OA cartilages when compared to that in normal cartilages.

3.7. Chondrocytes ferroptosis and EGFR downregulation occur during OA progression

We used DMM OA mouse model to investigate the expression of GPX4, a ferroptosis biomarker, and EGFR during the progression of OA. Safranin O/Fast Green staining showed the cartilages in DMM group exhibited a certain degree of degeneration, including proteoglycan loss, and cartilage destruction (Fig. 7A). The OARSI score of DMM group was significantly increased compared to the Sham group (Fig. 7D). Immunofluorescence staining showed that the number of GPX4 positive cells was decreased in the DMM group in comparison to that in Sham group, indicating ferroptosis is occurred during OA progression (Fig. 7B&E). Moreover, the expression of EGFR was also downregulated in DMM group (Fig. 7C&E). Collectively, these findings suggested a potential inverse correlation between chondrocytes ferroptosis and EGFR expression in the pathogenesis of OA.

3.8. Erastin induces chondrocytes ferroptosis, ECM degradation, and inhibits EGFR expression

Erastin is one of the commonly used inducer of ferroptosis [18]. The chemical structure of erastin is shown in Fig. 8A. Subsequently, chondrocytes were treated with different concentrations of erastin. As shown in Fig. 8B, the cell viability of chondrocytes was reduced in a dose-dependent manner. DCFH-DA and C11 BODIPY fluorescent probe were used to detect the level of intracellular ROS and lipid-ROS, respectively. The results showed that the intracellular ROS and lipid-ROS were increased after stimulated with 1 μM erastin (Fig. 8C&D). Moreover, we observed significant ultrastructure changes of mitochondria and decreased expression of GPX4 in erastin

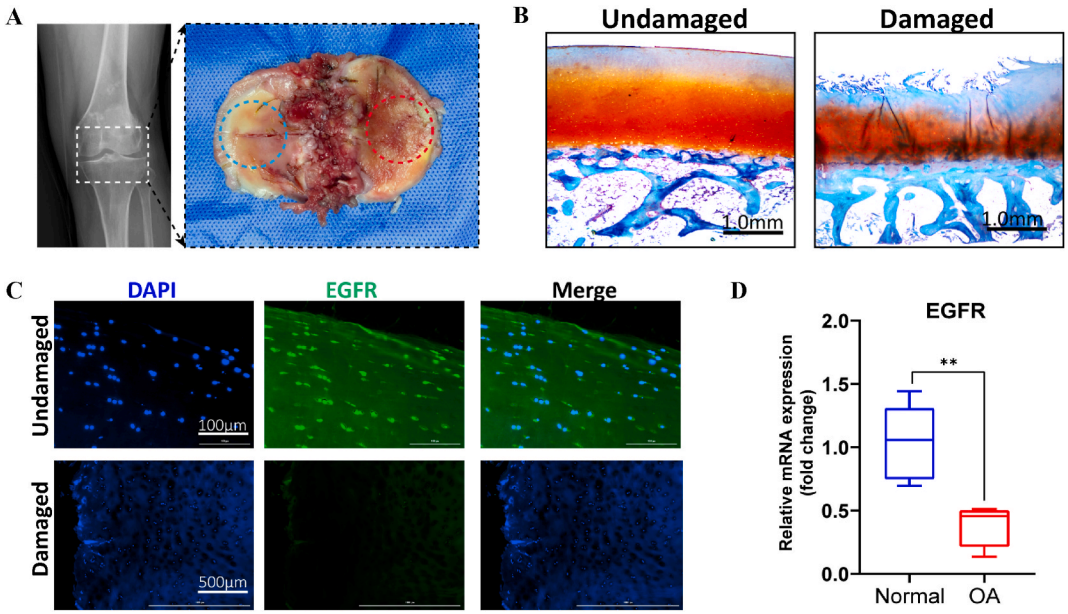

Fig. 6. The expression of EGFR in human normal and OA cartilages. (**A**) X ray image and Knee cartilage obtained from a 61-year-old patient who underwent total knee arthroplasty. The undamaged (bule circle) and damaged (red circle) samples were obtained from the articular cartilage of one patient with OA. (**B**) Safranin O/Fast Green staining of undamaged and damaged samples. Scale bar, 100 μm. (**C**) Detection the expression of EGFR between undamaged and damaged samples by immunofluorescence staining. (**D**) mRNA expression of EGFR between normal (n = 5) and OA samples (n = 5). Results are shown as means ± SEM. $^{**}P < 0.01$.

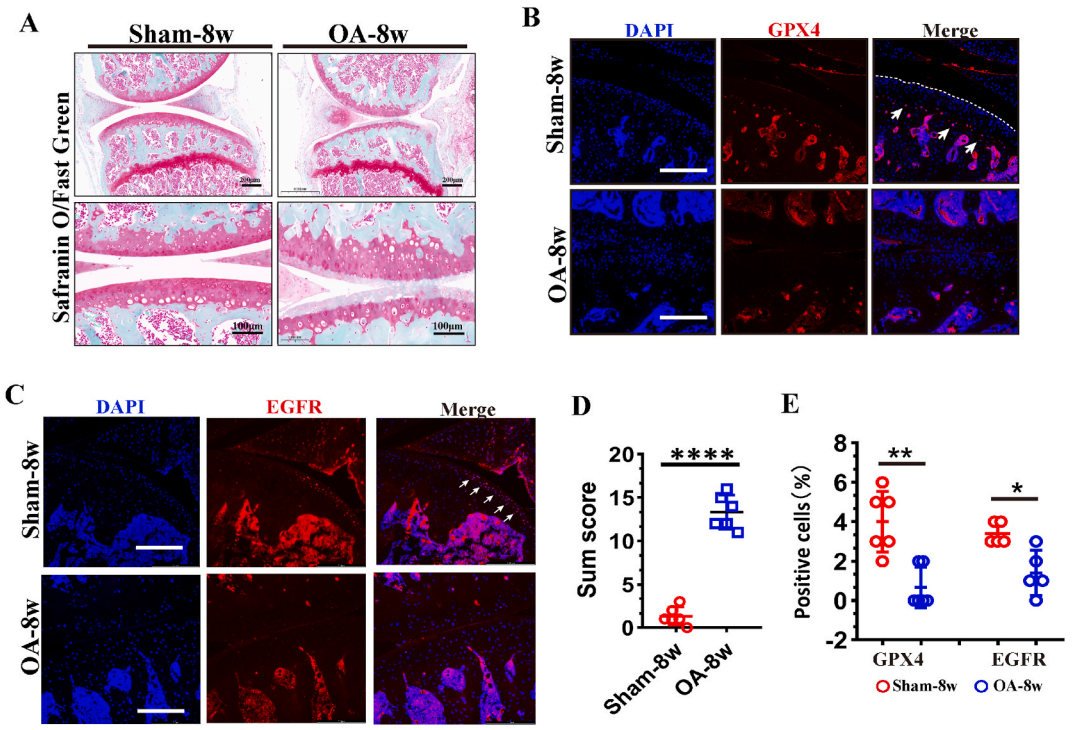

Fig. 7. Chondrocytes ferroptosis and EGFR downregulation occur during OA progression. (**A**) Safranin O/Fast Green staining of knee joints from contralateral sham samples and DMM samples at 8 weeks after surgery. Scale bar, 200 or 100 μm. (**B**) Immunofluorescence staining of GPX4. Scale bar, 100 μm. The white arrowheads show the positive cells of GPX4. (**C**) Immunofluorescence staining analysis of EGFR. Scale bar, 100 μm. The white arrowheads show the positive cells of EGFR. (**D**) Quantitative analysis of the OARSI score for the cartilage denegation. (**E**) Quantification of immunofluorescence analysis for GPX4 and EGFR (n = 6 for each group). Results are shown as mean ± SEM. $^{*}P < 0.05$, $^{**}P < 0.01$, $^{***}P < 0.001$, $^{****}P < 0.0001$.

treated chondrocytes (Fig. 8E–H). In addition, the results of qRT-PCR and Western blot showed that erastin decreased the level of collagen II and EGFR, and increased the production of MMP13 (Fig. 8F–H). Taking together, these findings indicated that ECM degradation, and EGFR downregulation occur as a result of chondrocytes ferroptosis.

3.9. EGFR inhibition promotes chondrocytes ferroptosis and ECM degradation

To further investigate the role of EGFR in chondrocytes ferroptosis and OA progression, gefitinib, one drug approved by Food and Drug Administration (FDA), was employed to inhibit the function of EGFR in chondrocytes. CCK-8 assay and toluidine blue staining were performed to evaluate the effect of various concentrations of gefitinib on chondrocytes. As shown in Fig. 9A, gefitinib at concentrations of 5, 10, 25, and 50 μM showed significant inhibition on the cell viability of chondrocytes. However, gefitinib at the concentration of 2.5 μM appeared to influence the growth of chondrocytes whereases there was no significant difference in comparison to control group. Chondrocytes incubated with gefitinib at the concentrations of 0, 2.5, 5, and 10 μM depicted little loss of coloration and unobvious morphological changes, while the concentration of 25 and 50 μM gefitinib could cause remarkable decrease of intercellular connections and cell number (Fig. 9B). Furthermore, the level of intracellular ROS and lipid-ROS in chondrocytes were accumulated after incubated with 10 μM gefitinib (Fig. 9C&D). The ultrastructural analysis showed that the mitochondria of gefitinib treated chondrocytes showed ruptured outer mitochondrial membrane, and reduced mitochondrial cristae (Fig. 9E). Furthermore, the results of qRT-PCR and western bolt demonstrated that gefitinib could suppress the expression of GPX4 (Fig. 9F–H). Meanwhile, the upregulation of MMP13 and downregulation of collagen II were observed in gefitinib treated chondrocytes (Fig. 9F–H). As an efficient ferroptosis specific inhibitor, Ferrostatin-1(Fer-1) was further used to explore whether the performance of EGFR inhibition in chondrocytes was related to ferroptosis. The results showed Fer-1 was able to reverse the gefitinib induced downregulation of Collagen II and GPX4, and upregulation of MMP13 (Fig. 9I&J). Collectively, these results suggested that EGFR inhibition may contribute to chondrocytes ferroptosis and ECM degradation *in vitro*.

4. Discussion

OA is a common degenerative disease, and the loss of chondrocytes serves as characteristic pathological changes of OA. Previous studies have suggested that various forms of chondrocytes death can contribute to the progression of OA [19–21]. Hence, targeting

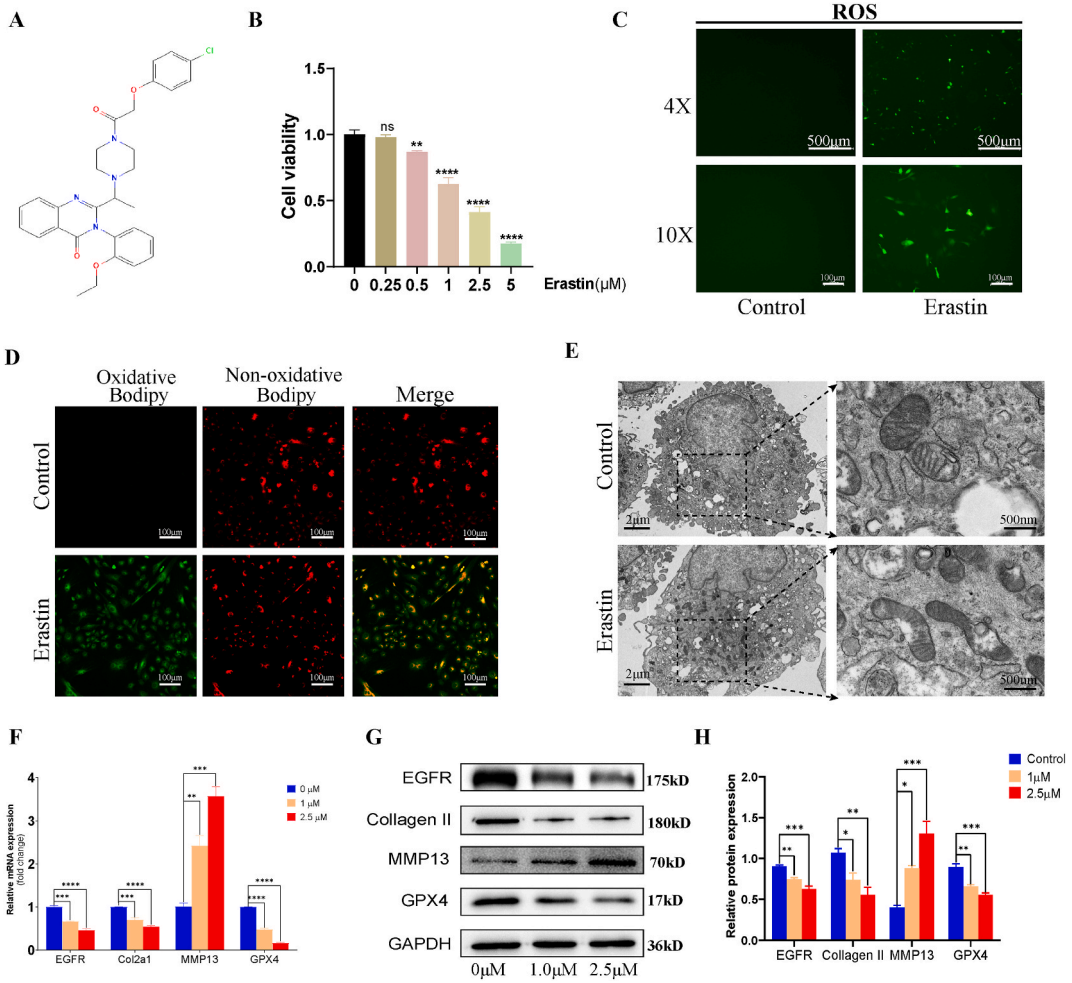

Fig. 8. Erastin induces chondrocytes ferroptosis, ECM degradation, and inhibits EGFR expression. (**A**) Chemical structure of erastin which was downloaded from https://pubchem.ncbi.nlm.nih.gov. (**B**) The effects of erastin (0, 0.25, 0.5, 1, 2.5, 5 μM) on the cell viability were determined by CCK-8 assay. (**C**) Intracellular ROS level detected by DCFH-DA. Scale bar: 4X, 500 μm; 10X, 100 μm. (**D**) Lipid-ROS level detected by C11 BODIPY fluorescent probe. Green, oxidized form of C11-BODIPY. Red, Non-oxidized form of C11-BODIPY. Scale bar, 100 μm. (**E**) The ultra-structures of mitochondria in chondrocytes treated with 0 or 1 μM erastin were observed using transmission electron microscopy. (**F**) The mRNA expression level of EGFR, Col2a1, MMP13, and GPX4 was examined by qRT-PCR. (**G**)The protein expression level of EGFR, Collagen II, MMP13, and GPX4 was examined by Western blot. (**H**) Relative protein expression was quantified by densitometry. GAPDH was used as the internal control. All experiments were repeated three times independently. All data are presented as the means ± SEM. *$P < 0.05$, **$P < 0.01$ ***$P < 0.001$, and ****P < 0.0001 versus Control group.

chondrocytes death has been regarded as an important approach for the treatment of OA [7,8]. Ferroptosis is defined as an iron- and ROS-dependent form of regulated cell death caused by the redox imbalance of oxidative and antioxidant systems [11,22]. Recent evidences indicated a close link between ferroptosis and OA [23]. Therefore, it is of significant importance to elucidate the function and mechanism of FRGs in chondrocytes ferroptosis, as this may lead to the identification of potential therapeutic targets for OA. In this study, comprehensive bioinformatics analyses were performed to identify ferroptosis-related biomarkers and their potential functions in the pathogenesis of OA using public GEO datasets and FerrDb database. Four genes including ACSF2, AURKA, EGFR and KLHL24 were identified as key DEFRGs which showed a robust performance in distinguishing OA and non-OA cartilage samples, and a possible correlation with the pathogenesis of OA. Importantly, EGFR, as a key DEFRG, was found decreased in human OA cartilages, OA mouse model, and erastin indued chondrocytes. Moreover, EGFR inhibition could accelerate chondrocytes ferroptosis and ECM degradation, which was reversed by the addition of Fer-1. Taking together, these findings suggested that the screened key DEFRGs may be involved in the molecular mechanisms of OA. Moreover, EGFR may function as an essential inhibitor in chondrocytes ferroptosis.

Recently, growing attention has been given to the role of ferroptosis in OA progression. It was shown that mechanical overload could induce chondrocytes ferroptosis through activating Piezo1 channel and subsequently facilitating calcium influx [21]. Treatment of chondrocytes with IL-1β stimulated the accumulation of intracellular Fe^{3+}, glutathione, ROS, malondialdehyde, and the upregulation of ferroptosis-related proteins [24]. Several genes have been found implicating in the pathogenesis of OA. For instance, the

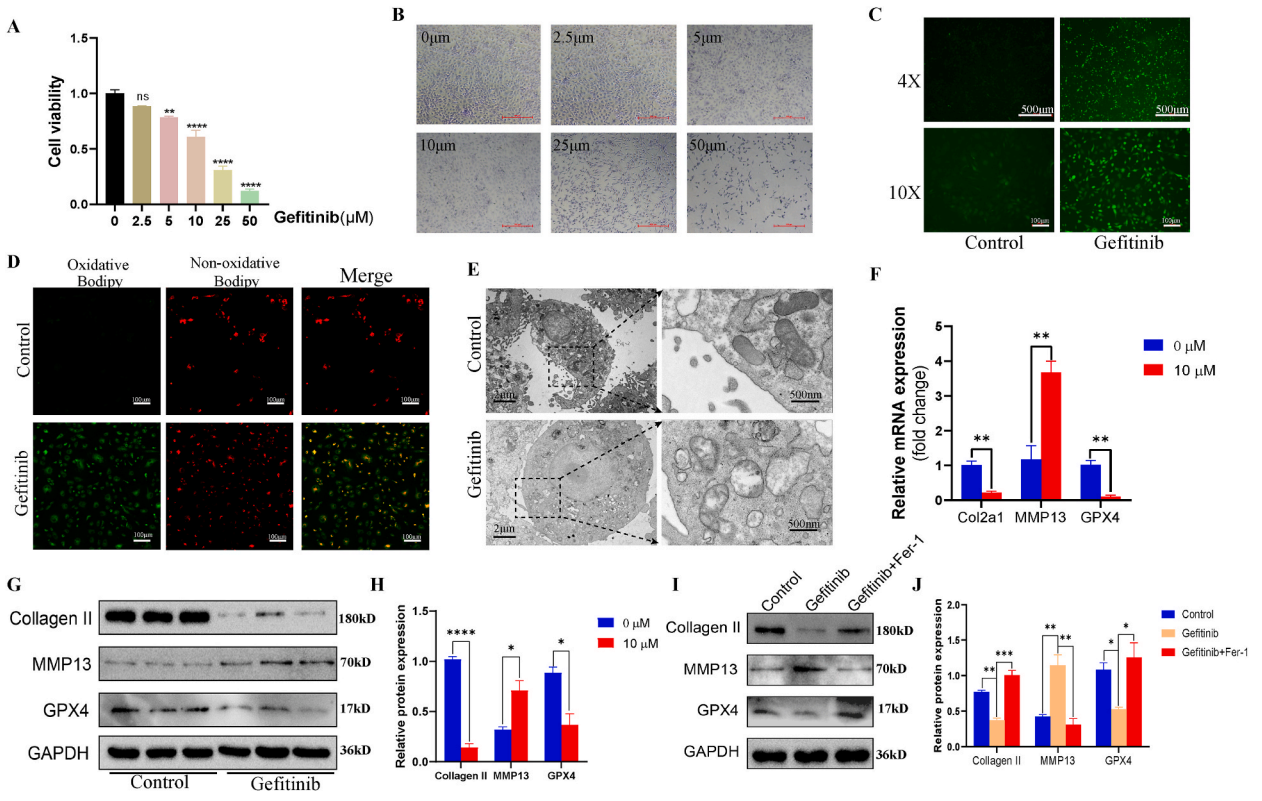

Fig. 9. Inhibition EGFR promotes chondrocytes ferroptosis and ECM degradation. (A) The effects of gefitinib (0, 2.5, 5, 10, 25, 50 μM) on the cell viability were determined by CCK-8 assay. (**B**) Toluidine blue staining showing the morphology of chondrocytes under various concentrations of gefitinib. (**C**) Intracellular ROS level detected by DCFH-DA. Scale bar: 4X, 500 μm; 10X, 100 μm. (**D**) Lipid-ROS level detected by C11 BODIPY fluorescent probe. Green, oxidized form of C11-BODIPY. Red, Non-oxidized form of C11-BODIPY. Scale bar, 100 μm. (**E**) The ultra-structures of mitochondria in chondrocytes treated with 0 or 10 μM gefitinib were observed using transmission electron microscopy. (**F**) The mRNA expression level of EGFR, Col2a1, MMP13, and GPX4 was examined by qRT-PCR. (**G**)The protein expression level of EGFR, Collagen II, MMP13, and GPX4 was examined by Western blot. (**H**) Relative protein expression was quantified by densitometry. GAPDH was used as the internal control. (**I**) Fer-1 reversed the gefitinib induced downregulation of collagen II and GPX4, and upregulation of MMP13. The cells in the Gefitinib + Fer-1 group were first incubated with the medium containing Fer-1 (1 μM) for 24 h, and then were incubated with the medium containing gefitinib (10 μM) for 24 h. The protein expression level of EGFR, Collagen II, MMP13, and GPX4 was examined by Western blot. (**J**) Relative protein expression was quantified by densitometry. GAPDH was used as the internal control. All experiments were repeated three times independently. All data are presented as the means ± SEM. $^{*}P < 0.05$, $^{**}P < 0.01$ $^{***}P < 0.001$, and $^{****}P < 0.0001$.

expression of GPX4 in OA cartilages was significantly lower than that in undamaged cartilages, and its downregulation could enhance the sensitivity of chondrocytes to oxidative stress, and thus accelerate ECM degradation through the MAPK/NF-κB pathway [25]. The RNA-binding protein SND1 has been found promoting the degradation of GPX4, thereby exacerbating inflammatory damage and ferroptosis of OA chondrocytes [26]. It was shown that NCOA4 was highly expressed in OA cartilages, and NCOA4 knockdown could attenuate IL-1β induced chondrocytes ferroptosis and ECM degradation [27]. In present study, a total of 42 DEFRGs were identified between the normal and OA cartilages. Significantly, these genes were mainly enriched in cell death related BPs, including the cellular response to oxidative stress, superoxide metabolic process, and positive regulation of programmed cell death. Meanwhile, these genes were primarily engaged in pathways of cartilage homeostasis and chondrocytes death, such as MAPK, PI3K-Akt, and mTOR signaling pathways [28–30]. Further ClueGO analysis revealed that ferroptosis was associated with the pathways of fat metabolism. It is reported that the metabolism of lipids regulates ferroptosis through controlling phospholipid peroxidation, as well as various other biological processes relevant to phospholipid peroxidation [31]. Hence, further investigation into DEFRGs may shed light on the molecular mechanisms of OA, and further provide therapeutic targets for OA treatment.

Several studies have indicated that bioinformatics analysis can help identify OA related biomarkers [32–34]. Liu et al. identified SLC3A2 as a potential therapeutic target of OA, and inhibition SLC3A2 could lead to chondrocytes ferroptosis and cartilage degeneration [32]. Xia et al. recognized seven FRGs, including ATF3, IL6, CDKN1A, IL1B, EGR1, JUN, and CD44, as the possible diagnostic biomarkers and targets for OA synovitis [33]. In addition, Wang et al. also found four FRGs including ATF3, TFRC, CXCL2 and JUN in synovial tissues between healthy controls and OA patients, which were also associated with the pathogenesis of chondrocytes ferroptosis [34]. In current study, a total of 10 candidate DEFRGs were subsequently identified. Our results showed that all candidate DEFRGs except GABPB1 and AURKA were down-regulated in OA cartilage samples. Furthermore, the expression treads of five

candidate DEFRGs, including ACSF2, AURKA, EGFR, KLHL24 and TUBE1, in GSE114007 dataset were found similar to those in GSE117999 dataset. It is known that ROC analysis is a useful tool for evaluating the performance of diagnostic tests and the accuracy of a statistical model [35]. It can be considered that AUC value greater than 0.5 indicates a certain diagnostic accuracy [36]. In this study, the AUC values of all DEFRGs were greater than 0.5 in both GSE117999 and GSE114007 datasets, suggesting that all candidate DEFRGs have certain diagnostic values in OA. Generally, the AUC of 0.7–0.8 is considered acceptable, 0.8 to 0.9 is considered excellent, and more than 0.9 is considered outstanding [35,36]. The AUC values of candidate DEFRGs including ACSF2, AURKA, EGFR, and KLHL24 were greater than 0.7 in both GSE117999 and GSE114007 datasets, indicating these four key DEFRGs have favorable diagnostic values, and may therefore be used as potential biomarkers of OA.

Significantly, multiple studies have documented the involvement of these four key DEFRGs in human diseases. It was shown that ACSF2 was remarkably down-regulated in ulcerative colitis animals and cell models, which may be used as a potential biomarker for the diagnosis and treatment of ulcerative colitis [37]. Shi et al. found that inhibition of ACSF2 could induce mitophagy, restore mitochondrial function, and keep from ischemia reperfusion induced acute kidney injury [38]. AURKA, one member of serine/threonine kinases, has been demonstrated functioning as an important biomarker and target in multiple tumors [39–41]. Moreover, AURKA can serve as a ubiquitinase, and was found upregulated in the human OA tissues and cells. Further analysis demonstrated that AURKA could contribute to mitochondrial dysfunction and the onset of OA by degrading superoxide dismutase 2 through K48 ubiquitination [42]. EGFR is a type I receptor tyrosine kinase and along with its ligands, and associates with multiple cellular pathways including cell survival and growth. EGFR upregulation is thought to be the principal mechanism of activation in a variety of tumors [43,44]. In addition, several studies have confirmed that EGFR is involved in the development of bone and growth plate, and the progression of OA [45,46]. KLHL24 is an E3 ubiquitin ligase, and KLHL24 overexpression has been reported impairing skin wound healing through the degradation of vimentin, and inducing alopecia via disrupting the structure of follicle stem cells [47,48]. In order to determine more details of these four DEFRGs in OA, we further classified OA patients according to the expression level of these key DEFRGs using unsupervised clustering analysis. Our study confirmed that a total of 882 DEGs were identified between these two ferroptosis related patterns. GO analysis showed that these DEGs were mainly enriched in ECM metabolism, inflammation, and immune regulation. The alteration of ECM, inflammation, and immune cell infiltration is believed participating in the regulation of OA pathogenesis [49–51]. KEGG analysis indicated that these DEGs were mainly involved in pathways including Toll-like receptor, PI3K-Akt, and NF-κB signaling pathways, which have been wildly reported in cartilage degeneration [52–54]. Considering these findings, these key DEFRGs may be associated with the pathogenesis of OA though regulating the ECM degradation, inflammation, and immune response.

CeRNAs have been reported involving in chondrocytes survival, ECM metabolism, inflammatory responses, and angiogenesis via post-transcriptional regulation [55,56]. Hence, a ceRNA network was created to search for lncRNAs and miRNAs that could function as the upstream regulators of these key DEFRGs. Interestingly, only EGFR was identified as the core gene to construct the ceRNA network. Significantly, a total of 3 lncRNAs and 4 miRNAs were screened to competitively regulate the expression of EGFR, respectively. Among these ceRNA networks, only LINC00265 has been demonstrated to promote the expression of EGFR in the tumorigenesis of colorectal cancer [57]. Several studies have shown that LINC00265 was implicated in the tumorigenesis of various cancers, such as hepatocellular carcinoma, bladder cancer, and gastric cancer [57–59]. Furthermore, Zou et al. reported that LINC00265 could contribute to chondrocytes apoptosis via sponging miR-101–3p, indicating that LINC00265 may serve as an important regulator in cartilage degeneration [60]. However, no studies have demonstrated the role of KCTD21-AS1 and LINC00051in human diseases yet. In addition, GO analysis showed that EGFR was associated with ferroptosis related BPs including cellular response to oxidative stress, cellular response to lipid, and negative regulation of programmed cell death. Meanwhile, EGFR has been found involved in OA related pathways such as FoxO, MAPK, and PI3K-Akt signaling pathways. Hence, we believe that these lncRNA-miRNA-EGFR networks may have the ability to regulate chondrocytes ferroptosis, thereby participating in the onset and development of OA.

EGFR, a 170-kDa kinase receptor, is expressed in most human tissues, including articular cartilage. It activates a cascade of downstream signaling pathways, including PI3K/Akt and MEK/MAPK pathways, and thus regulates abundant cellular processes such as cell proliferation, survival, and differentiation [61]. Previous studies have shown that EGFR was critical for maintaining the superficial layer of articular cartilage and cartilage homeostasis [62,63]. Mitogen-inducible gene 6 (Mig-6) is identified as a negative regulator of the EGFR, and its overexpression could cause an OA-like phenotype and earlier OA in mice [64]. Activating EGFR mediated signaling pathways is believed to attenuate posttraumatic OA following loading and surgical injury in mice [65,66]. These findings indicate that EGFR may function as a promising target of OA treatment. Meanwhile, some studies also suggested a link between EGFR and ferroptosis. For instance, it was shown that QSOX1 inhibited EGFR signal activation by enhancing ubiquitination-mediated degradation of EGFR, leading to sorafenib induced ferroptosis of hepatocellular carcinoma cells [67]. The ferroptosis inducer RSL3 showed a synthetic role with EGFR inhibitor, Cetuximab, to exacerbate the ferroptosis of nasopharyngeal carcinoma cells [68]. However, no studies have investigated the role of EGFR in chondrocytes ferroptosis. In current study, bioinformatic analyses showed EGFR was not only associated with OA progression, but also involved in the regulation of ferroptosis. Hence, these evidences appeared to indicate that EGFR may be involved in the progression of OA though regulating chondrocytes ferroptosis.

To further confirm the above hypothesis, *in vivo* and *in vitro* experiments were performed to identify the association between EGFR and chondrocytes ferroptosis. The protein level of EGFR appeared to be downregulated in damaged cartilage when compared to that in undamaged cartilage. Compared with normal cartilages, the mRNA level of EGFR was remarkably decreased in OA cartilages. Moreover, the level of EGFR was also found reduced in knee cartilages of OA mouse model and erastin induced chondrocytes, indicating an inverse correlation between EGFR expression and chondrocytes ferroptosis. Considering the AUC values of EGFR greater than 0.8 in both GSE1179999 and GSE1140007 datasets, EGFR may serve as an important biomarker in pathogenesis of OA. Importantly,

we found that EGFR inhibition could increase the production of ROS and lipid-ROS, and contribute to the significant change of mitochondrial crista and membrane. Furthermore, EGFR inhibition decreased the expression of GPX4, and induced ECM degradation. Interestingly, Fer-1, an ferroptosis inhibitor, could reverse the effect of EGFR inhibition on chondrocytes. All the above results indicated that EGFR may be an essential regulator in the chondrocytes ferroptosis. However, the underlying mechanisms of EGFR in chondrocytes ferroptosis require further exploration.

Several limitations should be pointed out when interpreting the current results. First, Only Safranin O/Fast Green staining was adopted for histologic analysis of OA changes. The combination of radiography with histopathology such as micro-CT and H&E staining will be more valid to evaluate the severity of OA. Second, only GPX4, as one of the key ferroptosis related biomarkers, was used to evaluate the occurrence of ferroptosis in current study. More approaches such as iron ion detection will be useful to comprehensively evaluate chondrocytes ferroptosis. Third, many confounding factors such as different clinical stages, therapies and concomitant diseases may affect the expression level of genes during OA progression. The discrepancy of AUC values calculated based on different datasets may be attributed to these reasons. Fourth, the constructed ceRNA networks were evaluated only via bioinformatic prediction, and therefore the exact roles of these lncRNA-miRNA-EGFR networks in OA need to be further investigated through *in vivo* and *in vitro* experiments.

5. Conclusion

In summary, ACSF2, AURKA, EGFR, and KLHL24 were identified as key FRGs that could serve as potential biomarkers and therapeutic targets for OA. Moreover, both *in vivo* and *in vitro* experiments suggested that EGFR may play a critical role in regulating chondrocytes ferroptosis during the pathogenesis of OA.

Author contribution statement

Hong Sun: Performed the experiments; Analyzed and interpreted the data; Contributed reagents, materials, analysis tools or data; Wrote the paper. Guoxuan Peng: Performed the experiments; Analyzed and interpreted the data; Contributed reagents, materials, analysis tools or data. Kunhao Chen: Performed the experiments; Contributed reagents, materials, analysis tools or data. Zhilin Xiong, Yong Zhuang: Analyzed and interpreted the data. Miao Liu, Xu Ning: Contributed reagents, materials, analysis tools or data. Hua Yang: Conceived and designed the experiments; Analyzed and interpreted the data; Contributed reagents, materials, analysis tools or data. Jin Deng: Conceived and designed the experiments; Analyzed and interpreted the data; Wrote the paper.

Funding statement

Hua Yang was supported by Science and Technology Fund of Guizhou Science and Technology Department {QKH-ZK [2021] 391}; Health Commission of Guizhou Province {gzwkj2021-261}.Hong Sun was supported by Science and Technology Fund of Guizhou Science and Technology Department {QKH-ZK [2023] 344}; Health Commission of Guizhou Province {gyfynsfc-2021-12}; Graduate Scientific Research Fund project of Guizhou {YJSKYJJ [2021]157}.Professor Jin Deng was supported by National Natural Science Foundation of China {82260372}.Guoxuan Peng was supported by National Natural Science Foundation of China {82360420}; Doctor Start-up Fund of Affiliated Hospital of Guizhou Medical University {gyfybskj-2023-07}.

Data availability statement

Data included in article/supplementary material/referenced in article.

Datasets used in the study (GSE117999, GSE1140007) can be downloaded without restriction from the public GEO database. The websites are as follows: GSE117999: https://www.ncbi.nlm.nih.gov/geo/query/acc.cgi?acc=GSE117999. GSE1140007: https://www.ncbi.nlm.nih.gov/geo/query/acc.cgi?acc=GSE114007.

Declaration of competing interest

All authors declare that they have no known competing financial interests or personal relationships that could have appeared to influence the work reported in this paper.

Acknowledgements

The authors would like to express their gratitude to Mrs. Dongbing Cui, the laboratory director of Guizhou Provincial Key Laboratory of Regenerative Medicine, for her generous assistance and guidance of experiments.

Appendix A. Supplementary data

Supplementary data to this article can be found online at https://doi.org/10.1016/j.heliyon.2023.e19975.

References

[1] Q. Yao, X. Wu, C. Tao, et al., Osteoarthritis: pathogenic signaling pathways and therapeutic targets, Signal Transduct. Targeted Ther. 8 (1) (2023) 56.
[2] G.B.D. Disease, I. Injury, C. Prevalence, Global, regional, and national incidence, prevalence, and years lived with disability for 354 diseases and injuries for 195 countries and territories, 1990-2017, in: A Systematic Analysis for the Global Burden of Disease Study 2017, Lancet, vol. 392, 2018, pp. 1789–1858, 10159.
[3] M. Kloppenburg, F. Berenbaum, Osteoarthritis year in review 2019: epidemiology and therapy, Osteoarthritis Cartilage 28 (3) (2020) 242–248.
[4] L. Tong, H. Yu, X. Huang, et al., Current understanding of osteoarthritis pathogenesis and relevant new approaches, Bone Res 10 (1) (2022) 60.
[5] Y. Fujii, L. Liu, L. Yagasaki, et al., Cartilage homeostasis and osteoarthritis, Int. J. Mol. Sci. 23 (11) (2022) 6316.
[6] L. Zheng, Z. Zhang, P. Sheng, et al., The role of metabolism in chondrocyte dysfunction and the progression of osteoarthritis, Ageing Res. Rev. 66 (2021), 101249.
[7] J. Yang, S. Hu, Y. Bian, et al., Targeting cell death: pyroptosis, ferroptosis, apoptosis and necroptosis in osteoarthritis, Front. Cell Dev. Biol. 9 (2021), 789948.
[8] S. Liu, Y. Pan, T. Li, et al., The role of regulated programmed cell death in osteoarthritis: from pathogenesis to therapy, Int. J. Mol. Sci. 24 (6) (2023) 5364.
[9] J. Zhou, J. Qiu, Y. Song, et al., Pyroptosis and degenerative diseases of the elderly, Cell Death Dis. 14 (2) (2023) 94.
[10] S.J. Dixon, K.M. Lemberg, M.R. Lamprecht, et al., Ferroptosis: an iron-dependent form of nonapoptotic cell death, Cell 149 (5) (2012) 1060–1072.
[11] X. Jiang, B.R. Stockwell, M. Conrad, Ferroptosis: mechanisms, biology and role in disease, Nat. Rev. Mol. Cell Biol. 22 (4) (2021) 266–282.
[12] D. Tang, X. Chen, R. Kang, et al., Ferroptosis: molecular mechanisms and health implications, Cell Res. 31 (2) (2021) 107–125.
[13] A. Ferreira, T. Duarte, S. Marques, et al., Iron triggers the early stages of cartilage degeneration in vitro: the role of articular chondrocytes, Osteoarthritis and Cartilage Open 3 (2) (2021), 100145.
[14] X. Yao, K. Sun, S. Yu, et al., Chondrocyte ferroptosis contribute to the progression of osteoarthritis, J Orthop Translat 27 (2021) 33–43.
[15] Y. Wan, K. Shen, H. Yu, et al., Baicalein limits osteoarthritis development by inhibiting chondrocyte ferroptosis, Free Radic. Biol. Med. 196 (2023) 108–120.
[16] Y.M. Park, W.Y. Lee, Y.S. Lim, et al., New technique for preparing cartilage for intracordal injection: the freezing and grinding method, J. Voice 28 (4) (2014) 508–511.
[17] M. Gosset, F. Berenbaum, S. Thirion, et al., Primary culture and phenotyping of murine chondrocytes, Nat. Protoc. 3 (8) (2008) 1253–1260.
[18] A. Bartos, J. Sikora, Bioinorganic modulators of ferroptosis: a review of recent findings, Int. J. Mol. Sci. 24 (4) (2023) 3634.
[19] J.E. Dilley, A. Seetharam, X. Ding, et al., CAMKK2 Is Upregulated in Primary Human Osteoarthritis and its Inhibition Protects against Chondrocyte Apoptosis, Osteoarthritis Cartilage, 2023.
[20] T. Ebata, M.A. Terkawi, K. Kitahara, et al., Macrophage-derived extracellular vesicles trigger non-canonical pyroptosis in chondrocytes leading to cartilage catabolism in osteoarthritis, Arthritis Rheumatol. 75 (8) (2023) 1358–1369.
[21] S. Wang, W. Li, P. Zhang, et al., Mechanical overloading induces GPX4-regulated chondrocyte ferroptosis in osteoarthritis via Piezo1 channel facilitated calcium influx, J. Adv. Res. 41 (2022) 63–75.
[22] H.F. Yan, T. Zou, Q.Z. Tuo, et al., Ferroptosis: mechanisms and links with diseases, Signal Transduct. Targeted Ther. 6 (1) (2021) 49.
[23] Q. Ru, Y. Li, W. Xie, et al., Fighting age-related orthopedic diseases: focusing on ferroptosis, Bone Res 11 (1) (2023) 12.
[24] W. Xu, B. Zhang, C. Xi, et al., Ferroptosis Plays a Role in Human Chondrocyte of Osteoarthritis Induced by IL-1beta in Vitro, 2023, 19476035221142011. Cartilage.
[25] Y. Miao, Y. Chen, F. Xue, et al., Contribution of ferroptosis and GPX4's dual functions to osteoarthritis progression, EBioMedicine 76 (2022), 103847.
[26] M. Lv, Y. Cai, W. Hou, et al., The RNA-binding protein SND1 promotes the degradation of GPX4 by destabilizing the HSPA5 mRNA and suppressing HSPA5 expression, promoting ferroptosis in osteoarthritis chondrocytes, Inflamm. Res. 71 (4) (2022) 461–472.
[27] K. Sun, L. Hou, Z. Guo, et al., JNK-JUN-NCOA4 axis contributes to chondrocyte ferroptosis and aggravates osteoarthritis via ferritinophagy, Free Radic. Biol. Med. 200 (2023) 87–101.
[28] Y. Zhang, W. Liu, Z. Liu, et al., Daurisoline attenuates H(2)O(2)-induced chondrocyte autophagy by activating the PI3K/Akt/mTOR signaling pathway, J. Orthop. Surg. Res. 18 (1) (2023) 248.
[29] X. Wang, Z. Guo, J. Lin, et al., Indirubin protects chondrocytes and alleviates OA by inhibiting the MAPK and NF-kappaB pathways, Int. Immunopharm. 115 (2023), 109624.
[30] Y. Qu, Y. Shen, L. Teng, et al., Chicoric acid attenuates tumor necrosis factor-alpha-induced inflammation and apoptosis via the Nrf2/HO-1, PI3K/AKT and NF-kappaB signaling pathways in C28/I2 cells and ameliorates the progression of osteoarthritis in a rat model, Int. Immunopharm. 111 (2022), 109129.
[31] D. Liang, A.M. Minikes, X. Jiang, Ferroptosis at the intersection of lipid metabolism and cellular signaling, Mol. Cell. 82 (12) (2022) 2215–2227.
[32] H. Liu, Z. Deng, B. Yu, et al., Identification of SLC3A2 as a potential therapeutic target of osteoarthritis involved in ferroptosis by integrating bioinformatics, clinical factors and experiments, Cells 11 (21) (2022) 3430.
[33] L. Xia, N. Gong, Identification and verification of ferroptosis-related genes in the synovial tissue of osteoarthritis using bioinformatics analysis, Front. Mol. Biosci. 9 (2022), 992044.
[34] X. Wang, T. Liu, C. Qiu, et al., Characterization and role exploration of ferroptosis-related genes in osteoarthritis, Front. Mol. Biosci. 10 (2023), 1066885.
[35] K.H. Zou, A.J. O'Malley, L. Mauri, Receiver-operating characteristic analysis for evaluating diagnostic tests and predictive models, Circulation 115 (5) (2007) 654–657.
[36] J.N. Mandrekar, Receiver operating characteristic curve in diagnostic test assessment, J. Thorac. Oncol. 5 (9) (2010) 1315–1316.
[37] L. Luo, S. Zhang, N. Guo, et al., ACSF2-mediated ferroptosis is involved in ulcerative colitis, Life Sci. 313 (2023), 121272.
[38] H. Shi, H. Qi, D. Xie, et al., Inhibition of ACSF2 protects against renal ischemia/reperfusion injury via mediating mitophagy in proximal tubular cells, Free Radic. Biol. Med. 198 (2023) 68–82.
[39] P. Jung, D. Horst, T. Kirchner, et al., AURKA is a prognostic biomarker for good overall survival in stage II colorectal cancer patients, Pathol. Res. Pract. 235 (2022), 153936.
[40] D. Jiang, H. Chen, J. Cao, Y, et al., AURKA, as a potential prognostic biomarker, regulates autophagy and immune infiltration in nasopharyngeal carcinoma, Immunobiology 228 (2) (2023), 152314.
[41] F. Richard, M. De Schepper, M. Maetens, et al., Comparison of the genomic alterations present in tumor samples from patients with metastatic inflammatory versus non-inflammatory breast cancer reveals AURKA as a potential treatment target, Breast (2023) 476–480.
[42] C. Yang, D. You, J. Huang, et al., Effects of AURKA-mediated degradation of SOD2 on mitochondrial dysfunction and cartilage homeostasis in osteoarthritis, J. Cell. Physiol. 234 (10) (2019) 17727–17738.
[43] M.L. Uribe, I. Marrocco, Y. Yarden, EGFR in cancer: signaling mechanisms, drugs, and acquired resistance, Cancers 13 (11) (2021) 2748.
[44] E.D.S. Santos, K.A.B. Nogueira, L.C.C. Fernandes, et al., EGFR targeting for cancer therapy: pharmacology and immunoconjugates with drugs and nanoparticles, Int. J. Pharm. 592 (2021), 120082.
[45] M. Linder, M. Hecking, E. Glitzner, et al., EGFR controls bone development by negatively regulating mTOR-signaling during osteoblast differentiation, Cell Death Differ. 25 (6) (2018) 1094–1106.
[46] L. Qin, F. Beier, EGFR signaling: friend or foe for cartilage? JBMR Plus 3 (2) (2019), e10177, 3.
[47] Y. Liu, J. Cui, J. Zhang, et al., Excess KLHL24 impairs skin wound healing through the degradation of vimentin, J. Invest. Dermatol. 143 (7) (2023) 1289–1298.
[48] J. Cui, Q. Zhao, Z. Song, et al., KLHL24-mediated hair follicle stem cells structural disruption causes alopecia, J. Invest. Dermatol. 142 (8) (2022) 2079–2087.e8.
[49] U. Nedunchezhiyan, I. Varughese, A.R. Sun, et al., Obesity, inflammation, and immune system in osteoarthritis, Front. Immunol. 13 (2022), 907750.
[50] J.E. Woodell-May, S.D. Sommerfeld, Role of inflammation and the immune system in the progression of osteoarthritis, J. Orthop. Res. 38 (2) (2020) 253–257.
[51] M. Rahmati, G. Nalesso, A. Mobasheri, et al., Aging and osteoarthritis: central role of the extracellular matrix, Ageing Res. Rev. 40 (2017) 20–30.
[52] Y. Won, J.I. Yang, S. Park, et al., Lipopolysaccharide binding protein and CD14, cofactors of Toll-like receptors, are essential for low-grade inflammation-induced exacerbation of cartilage damage in mouse models of posttraumatic osteoarthritis, Arthritis Rheumatol. 73 (8) (2021) 1451–1460.

[53] J. Liu, S. Jia, Y. Yang, et al., Exercise induced meteorin-like protects chondrocytes against inflammation and pyroptosis in osteoarthritis by inhibiting PI3K/Akt/NF-kappaB and NLRP3/caspase-1/GSDMD signaling, Biomed. Pharmacother. 158 (2023), 114118.
[54] J. Lu, Z. Miao, Y. Jiang, et al., Chrysophanol prevents IL-1beta-Induced inflammation and ECM degradation in osteoarthritis via the Sirt6/NF-kappaB and Nrf2/NF-kappaB axis, Biochem. Pharmacol. 208 (2023), 115402.
[55] H. Kong, M.L. Sun, X.A. Zhang, et al., Crosstalk among circRNA/lncRNA, miRNA, and mRNA in osteoarthritis, Front. Cell Dev. Biol. 9 (2021), 774370.
[56] H. Sun, G. Peng, X. Ning, et al., Emerging roles of long noncoding RNA in chondrogenesis, osteogenesis, and osteoarthritis, Am J Transl Res 11 (1) (2019) 16–30.
[57] H. Ge, Y. Yan, C. Yue, et al., Long noncoding RNA LINC00265 targets EGFR and promotes deterioration of colorectal cancer: a comprehensive study based on data mining and in vitro validation, OncoTargets Ther. 12 (2019) 10681–10692.
[58] Y. Zhi, F. Sun, C. Cai, et al., LINC00265 promotes the viability, proliferation, and migration of bladder cancer cells via the miR-4677-3p/FGF6 axis, Hum. Exp. Toxicol. 40 (12_suppl) (2021) S434–S446.
[59] Z. Yang, X. OuYang, L. Zheng, et al., Long intergenic noncoding RNA00265 promotes proliferation of gastric cancer via the microRNA-144-3p/Chromobox 4 axis, Bioengineered 12 (1) (2021) 1012–1025.
[60] H. Zou, C. Lu, J. Qiu, Long non-coding RNA LINC00265 promotes proliferation, apoptosis, and inflammation of chondrocytes in osteoarthritis by sponging miR-101-3p, Autoimmunity 54 (8) (2021) 526–538.
[61] D. Holowka, B. Baird, Mechanisms of epidermal growth factor receptor signaling as characterized by patterned ligand activation and mutational analysis, Biochim. Biophys. Acta Biomembr. (2017) 1430–1435, 1859(9 Pt A).
[62] H. Jia, X. Ma, W. Tong, et al., EGFR signaling is critical for maintaining the superficial layer of articular cartilage and preventing osteoarthritis initiation, Proc. Natl. Acad. Sci. U. S. A. 113 (50) (2016) 14360–14365.
[63] Y. Wei, X. Ma, H. Sun, et al., EGFR Signaling Is required for maintaining adult cartilage homeostasis and attenuating osteoarthritis progression, J. Bone Miner. Res. 37 (5) (2022) 1012–1023.
[64] M. Bellini, M.A. Pest, M. Miranda-Rodrigues, et al., Overexpression of MIG-6 in the cartilage induces an osteoarthritis-like phenotype in mice, Arthritis Res. Ther. 22 (1) (2020) 119.
[65] T. Gui, Y. Wei, L. Luo, et al., Activating EGFR signaling attenuates osteoarthritis development following loading injury in mice, J. Bone Miner. Res. 37 (12) (2022) 2498–2511.
[66] Y. Wei, L. Luo, T. Gui, et al., Targeting cartilage EGFR pathway for osteoarthritis treatment, Sci. Transl. Med. 13 (576) (2021), eabb3946.
[67] J. Sun, C. Zhou, Y. Zhao, et al., Quiescin sulfhydryl oxidase 1 promotes sorafenib-induced ferroptosis in hepatocellular carcinoma by driving EGFR endosomal trafficking and inhibiting NRF2 activation, Redox Biol. 41 (2021), 101942.
[68] S. Liu, S. Yan, J. Zhu, et al., Combination RSL3 treatment sensitizes ferroptosis- and EGFR-inhibition-resistant HNSCCs to Cetuximab, Int. J. Mol. Sci. 23 (16) (2022), 9014.